



Simulated Transcatheter Aortic Valve Flow: Implications of Elliptical Deployment and Under-Expansion at the Aortic Annulus

*Eric Sirois, †Wenbin Mao, *Kewei Li, *Joseph Calderan, and *†Wei Sun 

*Tissue Mechanics Laboratory, Biomedical Engineering Department and Department of Mechanical Engineering, University of Connecticut, Storrs, CT; and †The Wallace H. Coulter Department of Biomedical Engineering, Georgia Institute of Technology and Emory University, Atlanta, GA, USA

Abstract: Clinical use of transcatheter aortic valves (TAVs) has been associated with abnormal deployment, including oval deployment and under-expansion when placed into calcified aortic annuli. In this study, we performed an integrated computational and experimental investigation to quantify the impact of abnormal deployment at the aortic annulus on TAV hemodynamics. A size 23 mm generic TAV computational model, developed and published previously, was subjected to elliptical deployment at the annulus with eccentricity levels up to 0.68 and to under-expansion of the TAV at the annulus by up to 25%. The hemodynamic performance was quantified for each TAV deployment configuration. TAV opening geometries were fabricated using stereolithography and then subjected to steady forward flow testing in accordance with ISO-5840. Centerline pressure profiles were

compared to validate the computational model. Our findings show that slight ellipticity of the TAV may not lead to degeneration of hydrodynamic performance. However, under large ellipticity, increases in transvalvular pressure gradients were observed. Under-expanded deployment has a much greater negative effect on the TAV hemodynamics compared with elliptical deployment. The maximum turbulent viscous shear stress (TVSS) values were found to be significantly larger in under-expanded TAVs. Although the maximum value of TVSS was not large enough to cause hemolysis in all cases, it may cause platelets activation, especially for under-expanded deployments. **Key Words:** Transcatheter aortic valve—Replacement—Elliptical valve deployment—Computational simulation—Hemodynamics.

Transcatheter aortic valve replacement (TAVR) is a less invasive treatment for patients with severe aortic stenosis (AS) (1). It has been established as a standard of care in AS patients with high risk of surgical mortality or who are not suitable for surgery (2,3). Since the first-in-human implantation by Cribier et al. (4) in 2002, more than 150 000 patients worldwide (5,6) have benefited from this

revolutionary procedure. Recently, this therapy has been approved by Food and Drug Administration to treat intermediate-risk patients (7), with the advantages of less trauma and shorter recovery time.

For patients with AS, heavy calcium deposition on the valve leaflets and the aortic root can cause distortion of TAV geometries, resulting in a valve of an elliptical shape instead of a nominal circular shape. The geometrical assessment of elliptical TAV implantation with the self-expanding Core-Valve ReValving system was first reported by Schultz et al. (8). A recent study (9) also found noncircular deployment of the Lotus Valve System (Boston Scientific). An eccentricity index (defined as $1 - D_{\min}/D_{\max}$ where D_{\min} and D_{\max} are minimum and maximum TAV diameters after

doi: 10.1111/aor.13107

Received June 2017; revised November 2017; accepted December 2017.

Address correspondence and reprint requests to Wei Sun, Wallace H. Coulter Department of Biomedical Engineering, Georgia Institute of Technology, Technology Enterprise Park, Room 206, 387 Technology Circle, Atlanta, GA 30313, USA. E-mail: wei.sun@bme.gatech.edu

deployment, respectively) greater than 0.44 was identified in 25% of the patients with largest eccentricity index of 0.59. Valve under-expansion was also observed in 25% of the patients. In addition, geometrical measurement of the aortic annulus by multidetector computed tomography also revealed elliptical-shaped TAV deployment with the balloon expandable valves (10,11). Such an elliptical or under-expanded TAV configuration may disrupt blood flow through the valve, leading to high transvalvular gradients, energy loss, or other undesirable flow conditions. These undesirable conditions may increase the fluid shear stresses downstream of the TAV which in turn could lead to an increased risk of hemolysis (12).

Effects of elliptical and under-expanded TAV configurations on hemodynamics were not fully investigated and all previous studies were conducted by *in vitro* experiments. An experimental study (13) examined the fluid fields of circular and elliptical-shaped valves by particle image velocimetry. They reported that the elliptically shaped valve exhibited a higher fluid shear stress and turbulent kinetic energy downstream of the valve. However, the study only examined two cases and analyzed flow along a single plane. Another study (14) examined the hemodynamics of a custom-built TAV at circular, triangular, elliptical, and undersized configurations. They have reported that under-expanded valves have a significantly higher transvalvular gradient compared to the nominal condition. Furthermore, Scharfschwerdt et al. (15) examined the hemodynamics of the Edwards Sapien XT valve at circular, elliptical, triangular, and bulged configurations. A recent *in vitro* study (16) investigated the effects of the aortic annulus deformation and the leaflet thickness on the hydrodynamics of a homemade self-expanding TAV. They found that the triangular deformation produced the poorest valve function while the elliptical deformation led to the slightest difference from the nominal.

In this study, we developed an integrated computational and experimental approach to systematically analyze the impact of abnormal bioprosthetic aortic valve deployment on the valve hemodynamics. The degree of elliptical TAV configuration was measured from the clinical images of implanted transcatheter valves in patients. Finite element (FE) and computational fluid dynamics (CFD) simulations were performed to examine the structural and hemodynamic responses of TAVs at different configurations. A total of 27 computational simulations were performed to examine the abnormal TAVs

configurations through permutations of the following variables: degree of ellipticity, ellipticity at annulus or uniform throughout valve length, rotation of commissures, and annular constriction.

MATERIALS AND METHODS

Material properties

Glutaraldehyde-treated bovine pericardium (BP) is one of the biomaterials commonly used in the fabrication of TAVs (17). We have reported planar biaxial mechanical properties of thin BP (18). A generalized Fung-type elastic model (19) was utilized to characterize the thin BP mechanical behavior:

$$W = \frac{c}{2} [e^Q - 1], \quad (1)$$

$$Q = A_1 E_{11}^2 + A_2 E_{22}^2 + 2A_3 E_{11} E_{22} + A_4 E_{12}^2 + 2A_5 E_{11} E_{12} + 2A_6 E_{22} E_{12}$$

where c and $A_i = 1, 2, \dots, 6$ are material constants. The mean tissue thickness of 0.24 mm was adopted based on our measurements (18).

TAV geometry

The geometry of a nominal circular TAV has been described (18). To create geometries of elliptical TAV models, a circular TAV model was initially mounted on a stent which was simplified as a cylindrical tube. The degree of the elliptical TAV geometry was characterized by the eccentricity, which is the ratio of the distance between the two foci to the length of the major axis:

$$e = \sqrt{1 - \left(\frac{b}{a}\right)^2}, \quad (2)$$

where a and b are the lengths of the semimajor and semiminor axes of the ellipse, respectively. The eccentricities of elliptical TAVs were determined based on the *in vivo* images of the TAV patients. A maximum eccentricity of 0.68 was measured from the images in Fig. 6 of (8). Thus, three different eccentricities were investigated: 0.3, 0.5, and 0.68, which are designated as e_1 , e_2 , and e_3 , respectively. Displacement-controlled FE simulations were performed to develop the elliptical-shaped TAV models from the nominal circular valve model (20).

As there are three leaflets in a TAV device, their relative positions to the major and minor axes of an

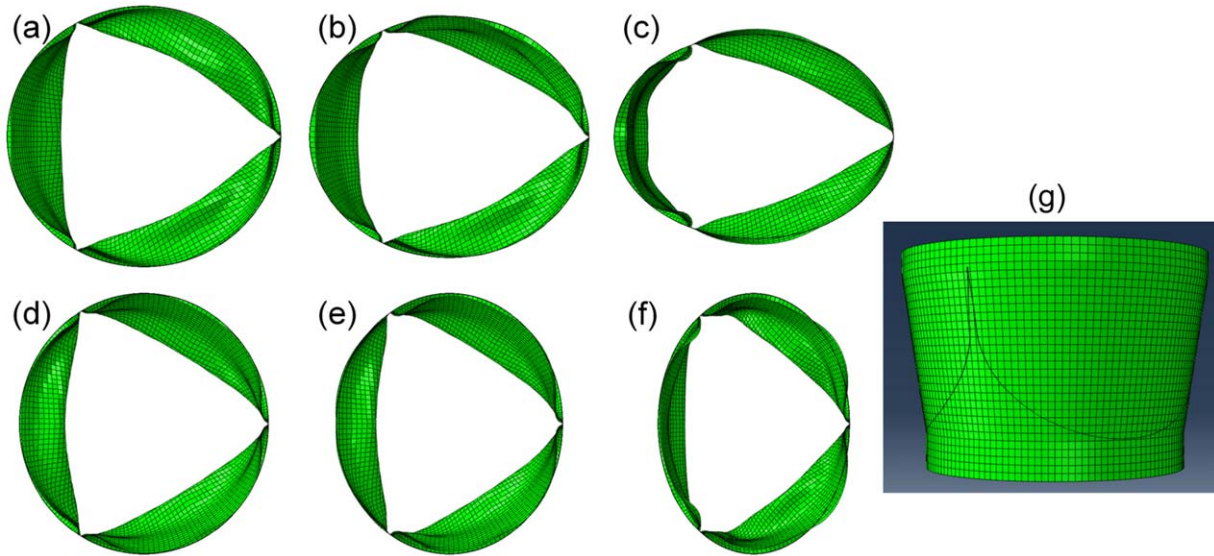


FIG. 1. Selected TAV models used in the simulations. (a) e1-r1-h1, (b) e2-r1-h1, (c) e3-r1-h1, (d) e1-r2-h1, (e) e2-r2-h1, (f) e3-r2-h1, (g) e0-c25. [Color figure can be viewed at wileyonlinelibrary.com]

elliptical TAV may have an impact on the deformed leaflet configuration. In this study, two orientations were investigated. For Scenario 1, the major axis was aligned with one of the three leaflet coaptation lines (Fig. 1a–c), which is denoted as “r1.” For Scenario 2, the major axis was perpendicular to the leaflet coaptation lines (Fig. 1d–f), which is denoted as “r2.” As there is a possibility that only one section of TAV device along the axial direction is deployed into the elliptical shape, we have created TAV models with uniform ellipticity from the TAV annulus to the TAV commissures, and also with ellipticity at the TAV annulus only (i.e., with a circular shape at the TAV commissures). These two scenarios are designated as “h1” and “h2,” respectively. For example, a TAV model with a uniform eccentricity of 0.30 through the whole stent height, and with the major axis aligned with the coaptation lines is named “e1-r1-h1” (Fig. 1b). Thus, we have created 12 elliptical TAV models. The nominal circular TAV model is denoted as “e0-c0.”

In addition, two cases of annular area constriction of 17%, denoted by “c17,” and 25%, or “c25,” with respect to the circular case were investigated (Fig. 1g). This scenario represents oversized valve used in TAV deployment. Two cases, “e0-c17” and “e0-c25,” were created such that the commissures of the valve were in a circular undistorted configuration. The two constricted annulus scenarios (with normal circularity at the commissures) were applied to the three ellipticity scenarios and two rotations to a total of additional 12 orientations. In total, 27 computational models were created.

Finite element model

Implementation of the Fung-elastic material model in ABAQUS (Dassault Systèmes SIMULIA Corp., Johnston, RI, USA) followed the methods previously established (21). Each leaflet has its own material orientations, which are described by the constitutive law of Eq. (1). The stiffer material orientation of the pericardium tissue was aligned with the circumferential direction of the leaflets; the less stiff orientation was aligned with the radial direction. The contact between each pair of leaflets was modeled by using a master-slave contact pair with the contact surfaces defined on the ventricular side of the leaflets. As the material of the stent is much stiffer than that of the leaflet, the deformation of the stent was neglected in this study. All the nodes on the leaflet-stent attachment contour lines were constrained in all three translational degrees of freedom. By applying a transvalvular pressure of 4 mm Hg to the ventricular side of the leaflets, a quasi-static approach was used to analyze the deformation of the TAV from the unloaded to the fully opened state.

Computational fluid dynamics model

To quantify the hemodynamics of TAVs in the opened position, the CFD software Star-CCM+ (CD-Adapco, Northville, MI, USA) was used. The guideline of ISO-5840 was followed for the steady forward flow testing of a prosthetic heart valve (appendix L.3) (22). Briefly, an incompressible fluid with a constant density of 1060 kg/m^3 and a viscosity of $0.0035 \text{ Pa} \cdot \text{s}$ was modeled in a

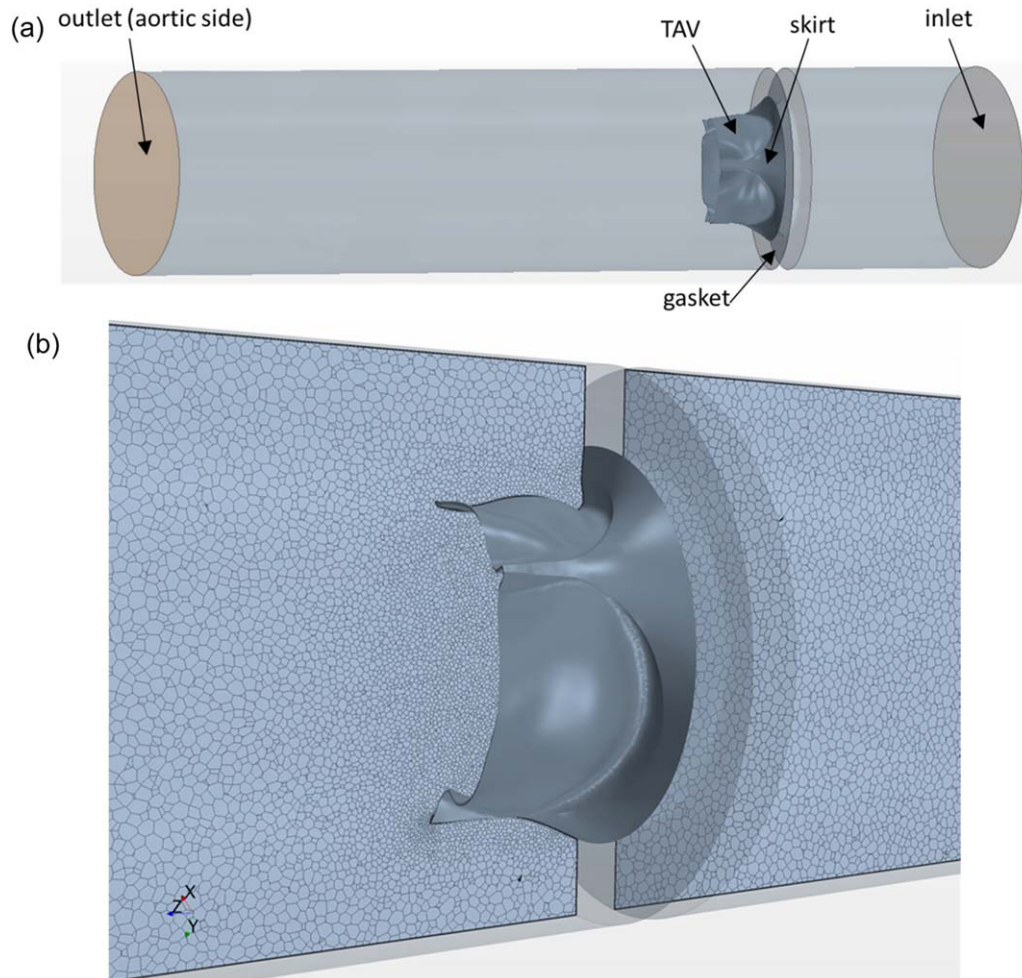


FIG. 2. (a) Three-dimensional CFD model for TAV simulations. (b) Polyhedral CFD mesh is shown in a bileaflet cross-sectional plane around TAV. [Color figure can be viewed at wileyonlinelibrary.com]

36.8 mm length tube. The valve was mounted centrally and sealed to the wall using a gasket (Fig. 2a). The inlet and outlet boundaries were 1.5 valve diameters upstream and five diameters downstream from the valve to prevent any boundary effects at the valve region. A polyhedral volume mesh was generated, with denser meshes used along the leaflet surfaces and at the joining of stent and gasket. The model was fully three-dimensional, containing approximately 1.3–1.4 million cells per model (Fig. 2b). Mesh convergence was performed to ensure the model fidelity. Turbulence modeling was performed using the realizable *k*-epsilon model (23). The turbulence intensity was set to 10% and the turbulent length scale was set to 3.5 mm. Following the ISO-5840 guidelines, a flow rate of 30 L/min was prescribed at the inlet and a constant pressure of 100 mm Hg was applied at the outlet.

In vitro experiment

The TAV geometries used in the CFD studies were replicated using stereolithography (Fig. 3). The valves were mounted into a custom-built steady flow loop. A centrifugal pump was used to create the flow conditions used in the CFD analysis. The test fluid was normal saline (0.9% NaCl) at body temperature (37°C). It has been reported that the viscosity of the fluid has a negligible effect on the transvalvular pressure drop and has been frequently used with pulse duplicators (14). The flow loop was comprised of long cylindrical sections before and after the mounting area of the valve to prevent excessive turbulence. Flow straighteners were used approximately 10 valve diameters upstream of the test section. A pressure transducer (World Precision Instruments, FL, USA) was used to record the centerline pressure of the fluid at 2 mm intervals starting one diameter upstream

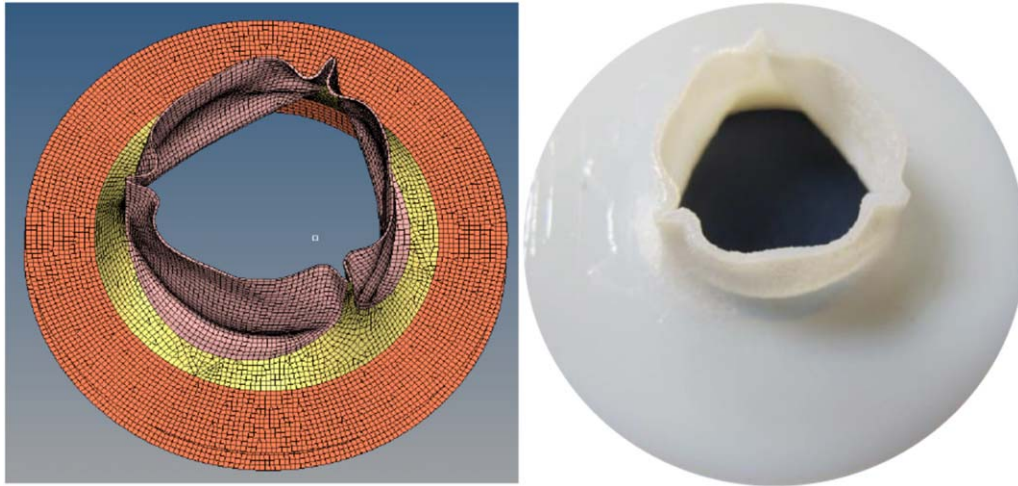


FIG. 3. CAD model of a TAV in the open configuration (left) and the corresponding fabricated stereolithography model (right). [Color figure can be viewed at wileyonlinelibrary.com]

of the valve to three diameters downstream of the annulus.

Definition of the calculated quantities

The following parameters were used to characterize hemodynamics through the valve: transvalvular pressure gradient (TPG) and turbulent viscous shear stress (TVSS). TPG was calculated as the pressure difference across the valve. TVSS has been correlated to blood cell damage in turbulent flow, which relates to turbulent dissipation rates which occur at Kolmogorov length scale (24). TVSS (25) can be calculated as $\tau_v = \sqrt{\rho\mu\epsilon/2}$, where μ is the dynamic viscosity of the fluid, ϵ is the turbulent dissipation rate (26).

RESULTS

Experimental validation

From Fig. 4a, it can be seen that the computational results and the experimental measurements of the valve centerline pressure follow similar trends. The region with the greatest discrepancy occurred immediately downstream of the valve. The simulated minimum centerline pressure for the circular TAV was 94 mm Hg at 22 mm downstream of the annulus. The experimental results showed a minimum pressure of 92.5 mm Hg at 20 mm downstream. Both the experimental and computational data showed consistent curves for the distance 24 mm and further downstream of the annulus.

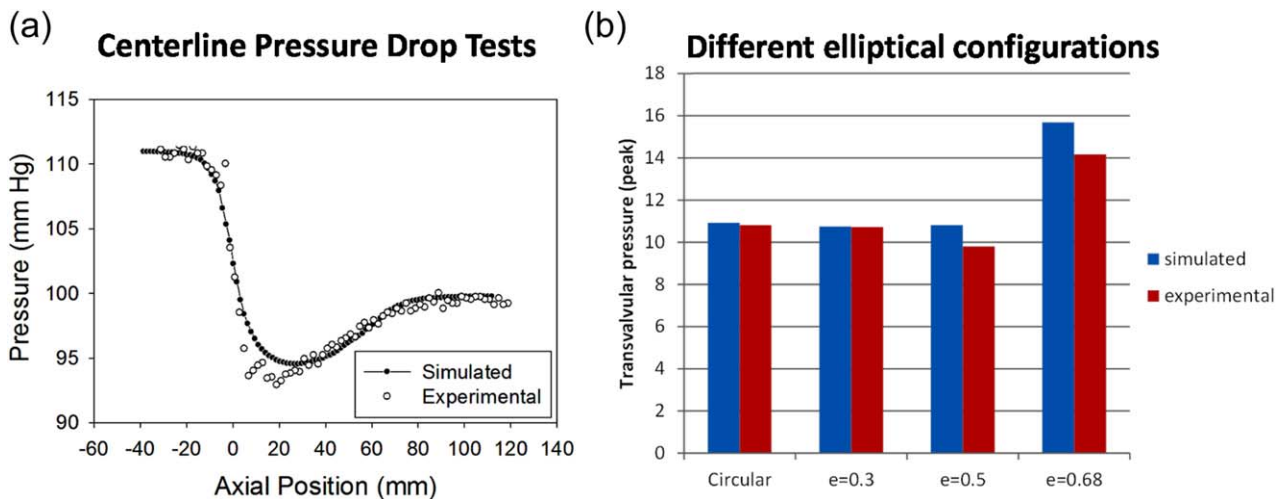


FIG. 4. (a) Centerline pressure drop comparison between simulation and experiment for the nominal circular case (e0-c0). (b) Comparison of simulated and experimental pressure drop for the cases: e0-c0, e1-r1-h1, e2-r1-h1, e3-r1-h1. [Color figure can be viewed at wileyonlinelibrary.com]

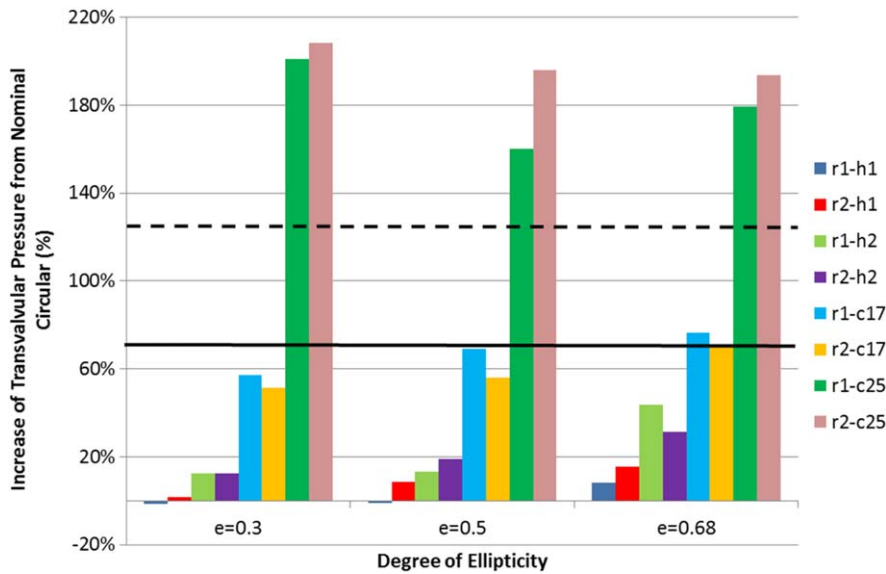


FIG. 5. The increase of transvalvular pressure gradient with respect to the nominal circular TAV for variations in ellipticity, orientation, annulus constriction, and height uniformity. The solid and dashed lines represent the results of scenario e0-c17 and e0-c25, respectively. [Color figure can be viewed at wileyonlinelibrary.com]

Figure 4b shows TPG for four cases with different ellipticity. The simulation results matched with the experiments.

Flow characteristics from CFD results

The impact of TAV configurations on the TPG is shown in Fig. 5. TPG generally increases with the increasing of TAV ellipticity, except for the scenario with severe under-expanded TAVs (r1-c25 and r2-c25). The baseline circular valve was found to have a peak transvalvular pressure gradient (PTPG) of 10.92 mm Hg, while the circular under-expanded valves of 17 and 25% (e0-c17 and e0-c25) had PTPGs of 18.54 mm Hg and 24.50 mm Hg, respectively. For valve deployment with mild ($e = 0.30$) or moderate ($e = 0.50$) ellipticity, PTPG was even smaller than that of the nominal circular valve (e.g., for cases of e1-r1-h1, e1-r2-h1, e2-r1-h1). Variation of ellipticity along the stent height (i.e., scenarios h1 and h2) had influences on valve performance as well. It was found that h2 scenarios had higher PTPGs than their h1 counterparts. TAV orientation had a minor effect on PTPG, where no optimal orientation for all situations was found. The change in PTPG was more pronounced under the annular constriction when compared to the change in ellipticity. The greatest increase of PTPG occurred at the largest annular constriction (25%) but with a mild ellipticity of $e = 0.30$.

Additionally, flow velocity contours were measured in a long-axis plane that passed through a valve commissure and bisected the other leaflet (plane 1), and a plane (plane 2) perpendicular to plane 1, as shown in Fig. 6. The nominal circular

valve (e0-c0) was found to have an almost symmetric center jet in plane 1 with a peak velocity of 2.16 m/s. The central jet in e0-c0 case propagated with the longest distance downstream, implying it had less energy dissipation loss, thus better hemodynamic performance. Based on the central jet length, hemodynamic performance of the remaining cases in descending order were e3-r2-h1, e3-r2-h2, e3-r1-h2, e0-c25, and e3-r1-c25. In general, the maximum velocity followed the same trend of PTPG, which the smallest velocity corresponding to the lowest PTPG. The central jets in plane 2 were more symmetric compared with the jets in plane 1 because the leaflet profiles were almost symmetric in plane 2. The large-scale features of the central jet were largely affected by the valve's geometry.

The vortices created by the central jet are represented using 3D streamlines in Fig. 7. For the nominal case, there were six vortex rings distributed almost axisymmetrically downstream of the valve. The same phenomena were observed for the under-expanded deployments (e.g., e0-c25, e3-r1-c25). However, the vortex rings were located closer to the centerline, creating smaller central jet orifices. In the cases of large ellipticity without under-expansion (e.g., e3-r1-h2), the vortex rings became irregular. The central flow was substantially confined, resulting in strong interaction between the vortex ring and the central jet downstream, as shown in Fig. 6. It is conjectured that smaller and less spread vortex rings decrease energy dissipation, leading to better hemodynamic performance.

The TVSS distribution, defined previously, is shown in Fig. 8. Generally, regions with high TVSS

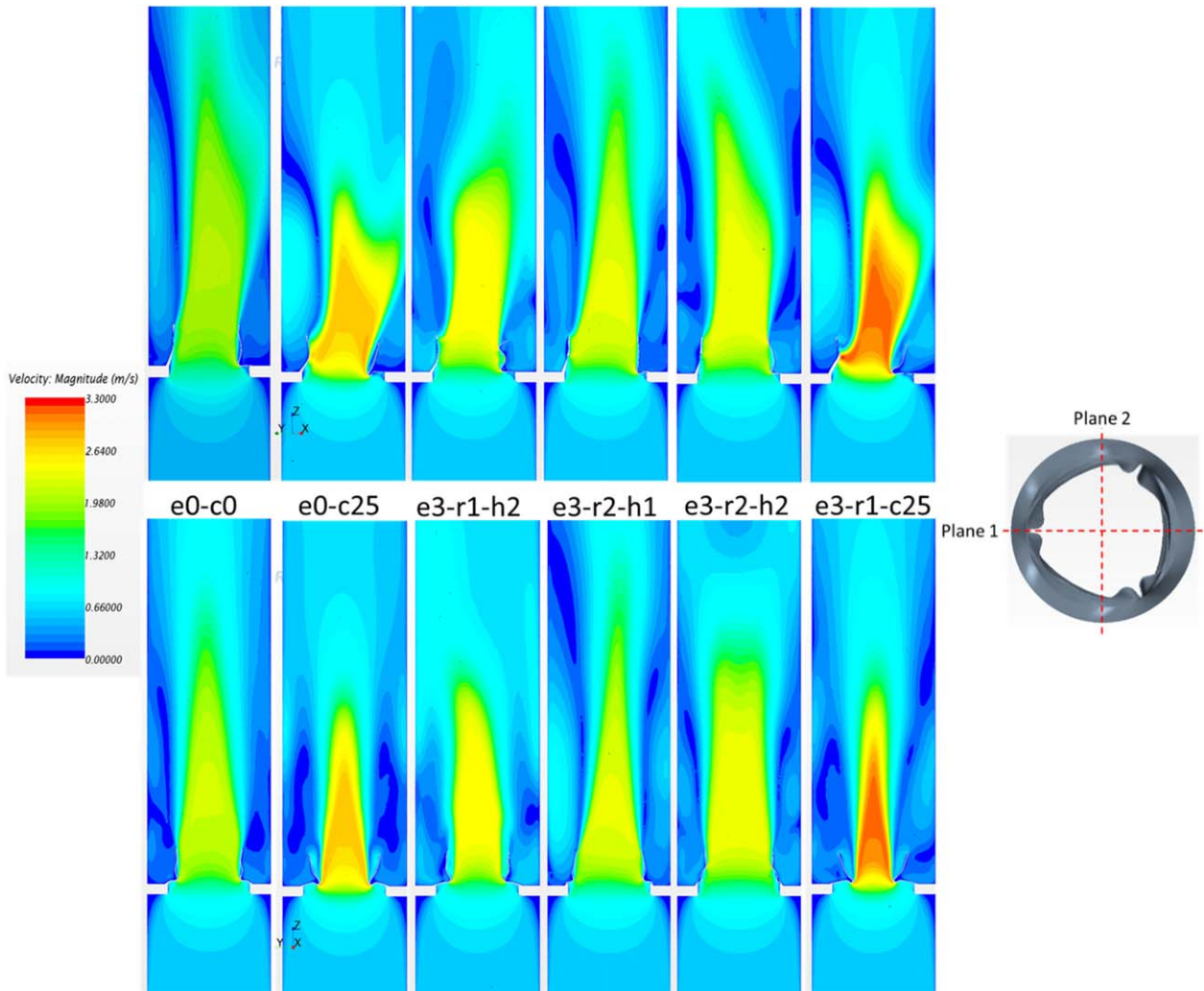


FIG. 6. Velocity contours in plane 1 (top) and plane 2 (bottom) for different valve deployments. [Color figure can be viewed at wileyonlinelibrary.com]

were observed in the shear layer region between the central jet and the edge of the leaflets, and also along the wake of the leaflets. Regions of high TVSS were expanded with increasing central jet velocity. Therefore, the cases of under-expansion had a larger area with elevated TVSS. The maximum values of TVSS in Fig. 8 were 13 Pa, 22 Pa, 16 Pa, 11 Pa, 11 Pa, 25 Pa, from the left to the right, respectively. Comparing elliptical without under-expansion cases to the nominal one, TVSS distributions were not significantly changed.

DISCUSSION

Although the TAV is designed for circular deployment, the TAV device landing zone often has a noncircular shape (27). The balloon-expandable Edwards SAPIEN valve often has a

mild elliptical shape after deployment, whereas the self-expandable CoreValve stent is soft, and thus may exhibit a stronger elliptical shape (28). The oversizing of TAVs has been commonly used clinically as a compromise to prevent the risk of the paravalvular leak. Therefore, the elliptical and under-expanded TAV deployment scenarios considered in this study provide a detailed investigation of different postdeployment configurations based on clinical evidence (8,9). It has been found that the ellipticity after deployment at different height levels of the TAV may not be the same (29,30). Thus, the deployment scenarios of h1 and h2 approximately represent this observation.

To our best knowledge, this study is the first to systematically analyze the impact of abnormal TAV deployment on the valve hemodynamics using an integrated computational and experimental

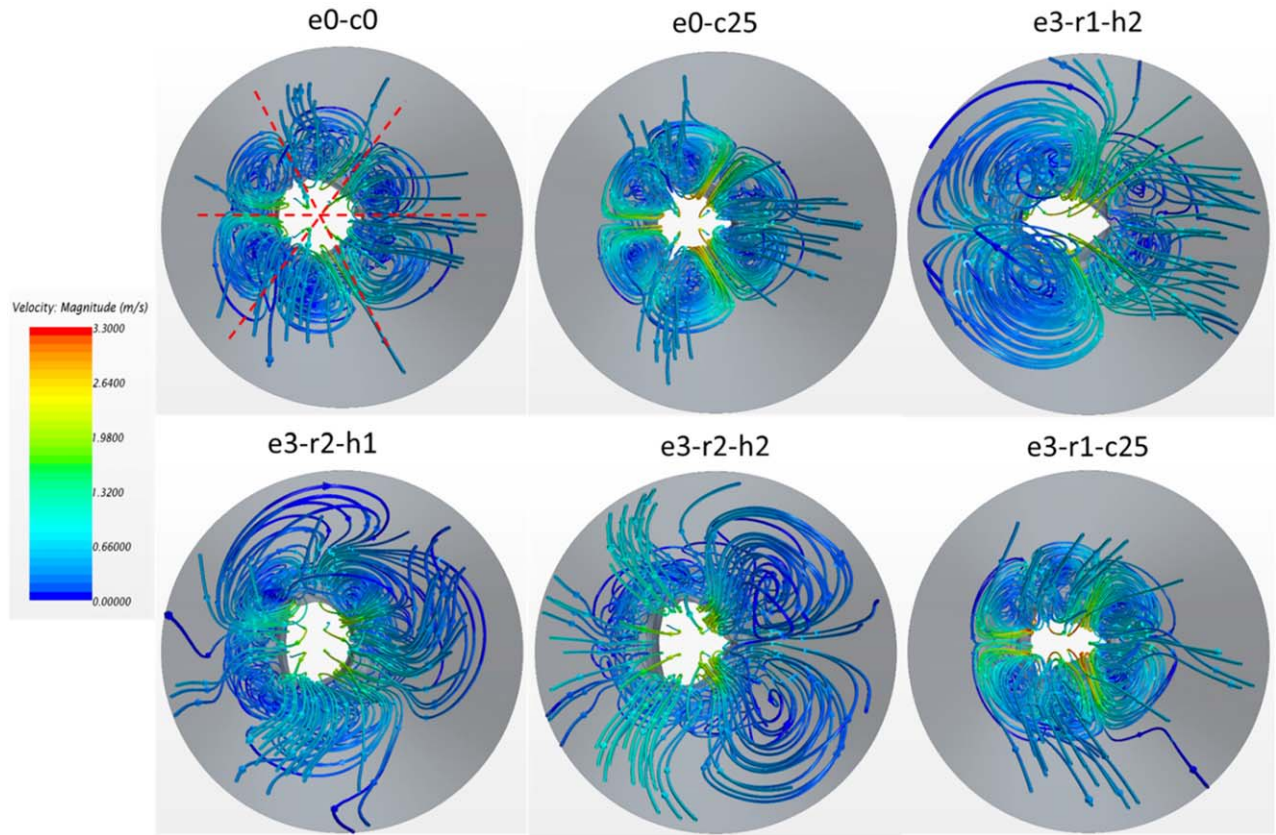


FIG. 7. 3D streamline patterns in top view for different valve deployments. The streamlines are colored by velocity magnitude. [Color figure can be viewed at wileyonlinelibrary.com]

approach. Although the effect of ellipticity and under-expanded deployment of TAVs on valvular hemodynamics has been studied previously by in vitro experiments (13–16,31,32), some of these studies have shown contradictory results due to the lack of parametric control. A study (13) found that the circular valve had a lower mean TPG compared with the elliptical valve for the test condition of 5 L/min CO (6.9 vs. 8.0 mm Hg). The eccentric valve used in this study is close to our e3-r2-h1 scenario. The increase of TPG is 16% compared with the circular case, which agrees well with an increase of 15% from our simulations. In another study, 26 mm noncommercial nitinol TAVs were deployed with four different configurations: circular, elliptical, triangular, and constricted circular geometries (14). Each configuration was tested in a half configuration, in which only the inflow portion of the valve was constrained (corresponding to “h2” scenarios), and in a full configuration (corresponding to “h1” scenarios). It was found that the circular valve had a higher TPG than elliptical configurations. As the eccentricity of the valve was not given, it is conjectured that the valve was deployed

into a slightly elliptical annulus. Therefore, smaller TPG in elliptical configurations can be explained by the results of our simulations for scenarios e1-r1-h1 and e2-r1-h1. Young et al. (14) also observed no significant difference between the half and full configurations in terms of TPG, whereas our simulations showed that “h1” configuration had a smaller PTPG than that of “h2” configuration. This may be explained by two reasons: (i) the stent shape at the commissure level in their half-configurations may not maintain a perfect circular shape as assumed in our h1 scenarios; and (ii) under slightly elliptical conditions, the difference in PTPG is small between the full and half-configurations, which is around 10% difference in our simulations (e.g., e1-r1-h1 vs. e1-r1-h2). In their experiment, the highly constricted circular configuration had a much large increase (more than 150%) in TPG compared to the nominal case, which agrees with our results (e0-c0 vs. e0-c25).

Kuettling et al. (31) investigated the influence of aortic annulus ovality on the hydrodynamics of the Medtronic CoreValve prostheses through in vitro experiment. They found that TVG increased with

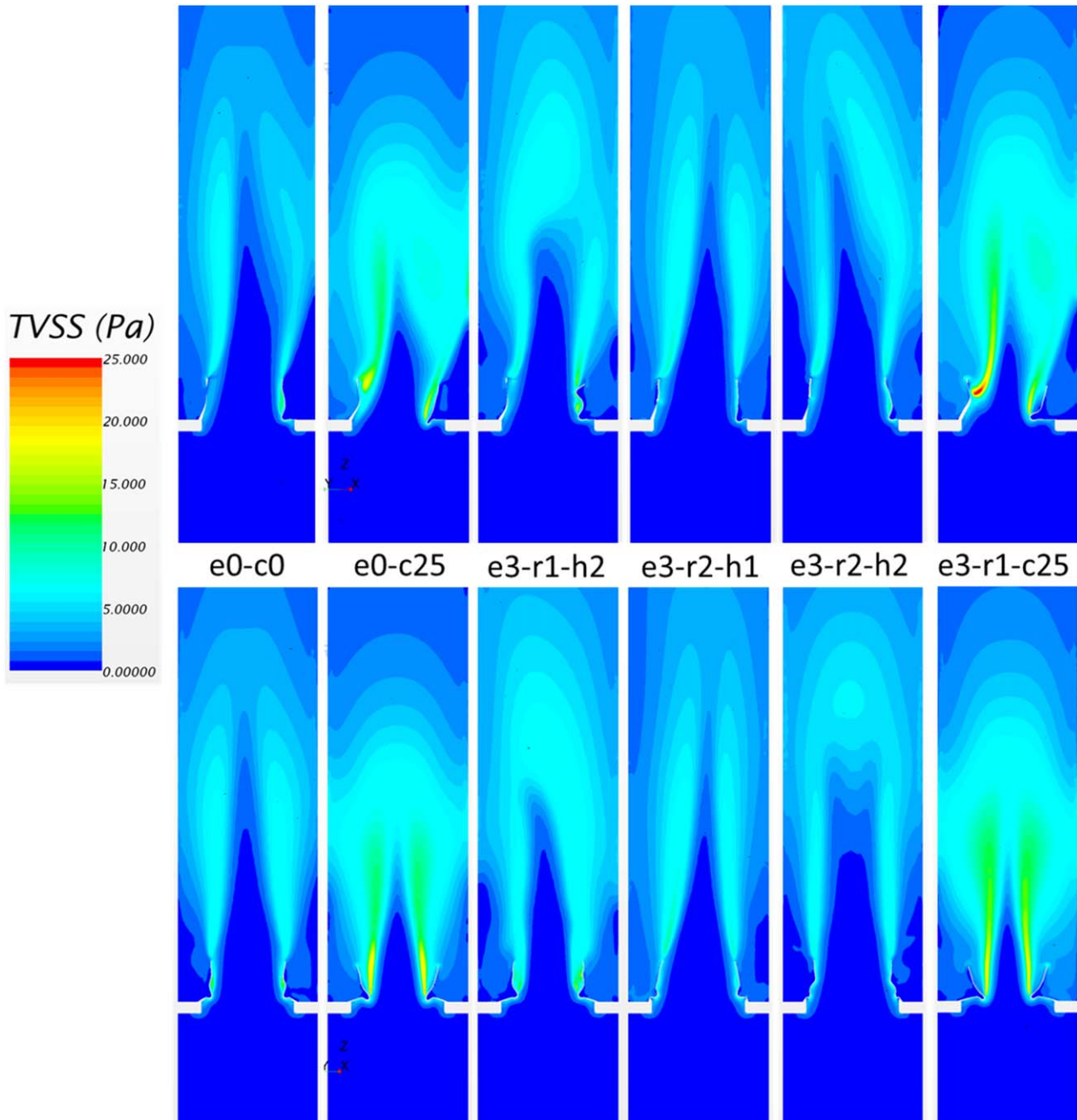


FIG. 8. Turbulent viscous shear stress contours in plane 1 (top) and plane 2 (bottom) for different valve deployments. [Color figure can be viewed at wileyonlinelibrary.com]

rising ellipticity and that more significant ovality lead to worsening of valve function and regurgitation. These findings are consistent with our results. The Edwards SAPIEN XT valve was also investigated in noncircular aortic annuli (15). It was reported that mean and peak TPGs were not influenced by the annulus configurations. By examining the annulus shape, it was found that the 24 mm artificial annuli used could cause a constriction of

15%. Therefore, their results can be compared to the scenarios of “c17” in our simulations. From our results, the e0-c17 case had a PTPG similar to the elliptical scenarios with the same degree of annular constriction. Again, our results agree with the experimental observations. Salaun et al. (32) investigated the effect of oversizing and elliptical shape on Edwards SAPIEN valves. They found that for a given aortic annulus area, mean TPGs were

generally lower with elliptical annuli compared to circular annuli. Interestingly, this observation can be partially explained by our results that under moderate under-expansion (“c17” scenarios), ellipticity may achieve a slightly better hydrodynamic performance compared with the circular case. This phenomenon is probably dependent on TAV leaflet design. In summary, the findings of this computational study are in accordance with several in vitro studies. The discrepancies in the experiments are mostly derived from the different degrees of under-expansion and ellipticity. However, based on the parametric study from well-controlled numerical simulations, these discrepancies can be explained.

In addition to the bulk hemodynamic criteria such as TPG, the detailed flow pattern and TVSS distribution were also examined. It is known that elevated levels of shear stresses may lead to hemolysis and thrombosis (33). Previously, hemolysis was thought to be caused by Reynolds shear stress (RSS) in turbulent flows (34). A more recent hypothesis suggests that TVSS at spatial scales similar to red blood cells are related to their damage (35,36). The threshold TVSS value for hemolysis in turbulent flows was found to be 60 Pa with a short exposure time of 0.012 ms (25), while the corresponding RSS threshold was 340 Pa. For the circular case, the maximum TVSS from our simulation is about 13 Pa, which is similar to a value of 12 Pa from an in vitro experiment (37). In all simulations, the TVSS values were smaller than 30 Pa, thus may not be sufficient to induce blood cell damage. Unlike red blood cells, platelets are more sensitive to shear stresses. It was reported the levels of TVSS in the range from 10 to 100 Pa can lead to platelet activation (33). Our results indicated that platelet activation may occur through the TAV during peak systole. However, if we consider the short exposure time due to the high velocity through the valve, the effect on platelet activation is yet to be confirmed.

Currently, there is substantial effort to expand TAVR to lower risk patients (38) after positive clinical results in intermediate risk patients. However, recent evidence of leaflet thrombosis in TAVs (39,40) has led to concerns of stroke and long-term valve durability. Although risk factors for thrombosis in TAVR patients remain poorly defined, recent data suggest that the hemodynamic environment in the vicinity of the TAV is a factor in the development of leaflet thrombosis (41–43). This environment can be altered by anatomical, procedural, and device related parameters, such as the elliptical deployment of TAV studied in this article. In the future, we hope

that the developed computational models can be combined with the established TAV fatigue model in our lab (44,45) to investigate the altered hemodynamics on leaflet thrombosis and TAV durability due to the suboptimal TAV developments.

There are some limitations in this study. Only one initial leaflet geometry was used to create the abnormal TAV models. Alternative initial leaflet geometries may generate different results (46,47). However, it is expected that the overall trends in pressure gradient and flow patterns will hold for different TAV designs. Another limitation was the use of a fully opened leaflet configuration in the steady forward flow. Therefore, transvalvular regurgitation during diastole cannot be studied. During a cardiac cycle, the valve leaflets interact with the fluid stream which could cause the leaflets to deform and affect the flow. Thus, the unsteady changes in flow may not be captured. More accurate flow simulations may be achieved with valve fluid–structure interactions (48) rather than retaining a fixed leaflet wall boundary.

CONCLUSION

We systematically investigated the effect of elliptical and under-expansion deployments on transcatheter aortic valve hemodynamics. The results of numerical simulations were compared to the in vitro experiment to verify the accuracy of numerical method. Our findings show that slight ellipticity of TAVs may not necessarily lead to degeneration of hydrodynamic performance. However, under large ellipticity, increases in transcatheter pressure gradient were observed. Under-expansion has a much greater negative effect on TAV hemodynamics than valve ellipticity. The maximum turbulent viscous shear stress values were found to be significantly larger in under-expanded TAVs, but these values were not large enough to cause hemolysis in all cases.

Acknowledgments: Research for this work was funded in part by NIH HL104080 and HL108240 grants. Technical support from Edwards Lifesciences and Dura Biotech was also gratefully acknowledged. Wenbin Mao was supported by an American Heart Association Postdoctoral Fellowship 15POST25910002.

REFERENCES

1. Webb JG, Chandavimol M, Thompson CR, et al. Percutaneous aortic valve implantation retrograde from the femoral artery. *Circulation* 2006;113:842–50.

2. Leon MB, Smith CR, Mack M, et al. Transcatheter aortic valve implantation for aortic stenosis in patients who cannot undergo surgery. *N Engl J Med* 2010;363:1597–607.
3. Smith CR, Leon MB, Mack MJ, et al. Transcatheter versus surgical aortic-valve replacement in high-risk patients. *N Engl J Med* 2011;364:2187–98.
4. Cribier A, Eltchaninoff H, Bash A, et al. Percutaneous transcatheter implantation of an aortic valve prosthesis for calcific aortic stenosis: first human case description. *Circulation* 2002;106:3006–8.
5. Blanke P, Schoepf UJ, Leipsic JA. CT in transcatheter aortic valve replacement. *Radiology* 2013;269:650–69.
6. Zhao Z-G, Jilalawi H, Feng Y, Chen M. Transcatheter aortic valve implantation in bicuspid anatomy. *Nat Rev Cardiol* 2015;12:123–8.
7. Cribier A. The development of transcatheter aortic valve replacement (TAVR). *Global Cardiol Sci Pract* 2017;2016.
8. Schultz CJ, Weustink A, Piazza N, et al. Geometry and degree of apposition of the CoreValve ReValving system with multislice computed tomography after implantation in patients with aortic stenosis. *J Am Coll Cardiol* 2009;54:911–8.
9. Gooley RP, Cameron JD, Meredith IT. Assessment of the geometric interaction between the lotus transcatheter aortic valve prosthesis and the native ventricular aortic interface by 320-multidetector computed tomography. *JACC Cardiovasc Interv* 2015;8:740–9.
10. Delgado V, Ng AC, van de Veire NR, et al. Transcatheter aortic valve implantation: role of multi-detector row computed tomography to evaluate prosthesis positioning and deployment in relation to valve function. *Eur Heart J* 2010;3:1114–23.
11. Willson AB, Webb JG, Labounty TM, et al. 3-dimensional aortic annular assessment by multidetector computed tomography predicts moderate or severe paravalvular regurgitation after transcatheter aortic valve replacement: a multicenter retrospective analysis. *J Am Coll Cardiol* 2012;59:1287–94.
12. Himbert D, Pontnau F, Messika-Zeitoun D, et al. Feasibility and outcomes of transcatheter aortic valve implantation in high-risk patients with stenotic bicuspid aortic valves. *Am J Cardiol* 2012;110:877–83.
13. Gunning PS, Saikrishnan N, McNamara LM, Yoganathan AP. An in vitro evaluation of the impact of eccentric deployment on transcatheter aortic valve hemodynamics. *Ann Biomed Eng* 2014;42:1195–206.
14. Young E, Chen JF, Dong O, Gao S, Massiello A, Fukamachi K. Transcatheter heart valve with variable geometric configuration: in vitro evaluation. *Artif Organs* 2011;35:1151–9.
15. Scharfschwerdt M, Meyer-Saraei R, Schmidtke C, Sievers HH. Hemodynamics of the Edwards Sapien XT transcatheter heart valve in noncircular aortic annuli. *J Thorac Cardiovasc Surg* 2014;148:126–32.
16. Feng W, Yang X, Liu Y, Fan Y. An in vitro feasibility study of the influence of configurations and leaflet thickness on the hydrodynamics of deformed transcatheter aortic valve. *Artif Organs* 2017;41:735–43.
17. Zajarias A, Cribier AG. Outcomes and safety of percutaneous aortic valve replacement. *J Am Coll Cardiol* 2009;53:1829–36.
18. Li K, Sun W. Simulated thin pericardial bioprosthetic valve leaflet deformation under static pressure-only loading conditions: implications for percutaneous valves. *Ann Biomed Eng* 2010;38:2690–701.
19. Fung YC. *Biomechanics: Mechanical Properties of Living Tissues*, 2nd Edition. New York: Springer Verlag, 1993.
20. Sun W, Li K, Sirois E. Simulated elliptical bioprosthetic valve deformation: implications for asymmetric transcatheter valve deployment. *J Biomech* 2010;43:3085–90.
21. Sun W, Sacks MS. Finite element implementation of a generalized Fung-elastic constitutive model for planar tissues. *Biomech Model Mechanobiol* 2005;4:190–9.
22. International Standards Organization. *ISO5840: Cardiovascular Implants—Cardiac Valve Prosthesis (Committee Draft)*. Geneva, Switzerland: International Standards Organization, 1994;18–24.
23. Sirois E, Sun W. Computational evaluation of platelet activation induced by a bioprosthetic heart valve. *Artif Organs* 2011;35:157–65.
24. Jones SA. A relationship between Reynolds stresses and viscous dissipation: implications to red cell damage. *Ann Biomed Eng* 1995;23:21–8.
25. Yen J-H, Chen S-F, Chern M-K, Lu P-C. The effect of turbulent viscous shear stress on red blood cell hemolysis. *J Artif Organs* 2014;17:178–85.
26. Morshed KN, Bark D Jr, Forleo M, Dasi LP. Theory to predict shear stress on cells in turbulent blood flow. *PLoS One* 2014;9:e105357.
27. Zegdi R, Ciobotaru V, Noghin M, et al. Is it reasonable to treat all calcified stenotic aortic valves with a valved stent? Results from a human anatomic study in adults. *J Am Coll Cardiol* 2008;51:579–84.
28. Schuhbaeck A, Weingartner C, Arnold M, et al. Aortic annulus eccentricity before and after transcatheter aortic valve implantation: comparison of balloon-expandable and self-expanding prostheses. *Eur J Radiol* 2015;84:1242–8.
29. Kazuno Y, Maeno Y, Kawamori H, et al. Comparison of SAPIEN 3 and SAPIEN XT transcatheter heart valve stent-frame expansion: evaluation using multi-slice computed tomography. *Eur Heart J Cardiovasc Imaging* 2016;17:1054–62.
30. Rodríguez-Olivares R, Rahhab Z, El Faquir N, et al. Differences in frame geometry between balloon-expandable and self-expanding transcatheter heart valves and association with aortic regurgitation. *Rev Esp Cardiol (Engl Ed)* 2016;69:392–400.
31. Kuetting M, Sedaghat A, Utzenrath M, et al. In vitro assessment of the influence of aortic annulus ovality on the hydrodynamic performance of self-expanding transcatheter heart valve prostheses. *J Biomech* 2014;47:957–65.
32. Salaun E, Zenses A-S, Evin M, et al. Effect of oversizing and elliptical shape of aortic annulus on transcatheter valve hemodynamics: an in vitro study. *Int J Cardiol* 2016;208:28–35.
33. Sutura SP. Flow-induced trauma to blood cells. *Circ Res* 1977;41:2–8.
34. Grigioni M, Daniele C, D’Avenio G, Barbaro V. A discussion on the threshold limit for hemolysis related to Reynolds shear stress. *J Biomech* 1999;32:1107–12.
35. Antiga L, Steinman DA. Rethinking turbulence in blood. *Biorheology* 2009;46:77–81.
36. Ge L, Dasi LP, Sotiropoulos F, Yoganathan AP. Characterization of hemodynamic forces induced by mechanical heart valves: Reynolds vs. viscous stresses. *Ann Biomed Eng* 2008;36:276–97.
37. Li C-P, Lo C-W, Lu P-C. Estimation of viscous dissipative stresses induced by a mechanical heart valve using PIV data. *Ann Biomed Eng* 2010;38:903–16.
38. Gravel GM, G en ereux P. Exploring the role of transcatheter aortic valve replacement as the preferred treatment for lower-risk patients. *J Am Coll Cardiol* 2015;66:1638.
39. De Marchena E, Mesa J, Pomenti S, et al. Thrombus formation following transcatheter aortic valve replacement. *JACC: Cardiovasc Interv* 2015;8:728–39.
40. Makkar RR, Fontana G, Jilalawi H, et al. Possible subclinical leaflet thrombosis in bioprosthetic aortic valves. *N Engl J Med* 2015;373:2015–24.
41. Egbe AC, Pislaru SV, Pellicka PA, et al. Bioprosthetic valve thrombosis versus structural failure: clinical and echocardiographic predictors. *J Am Coll Cardiol* 2015;66:2285–94.
42. Hansson NC, Grove EL, Andersen HR, et al. Transcatheter aortic valve thrombosis: incidence, predisposing factors, and clinical implications. *J Am Coll Cardiol* 2016;68:2059–69.
43. Leetmaa T, Hansson NC, Leipsic J, et al. Early aortic transcatheter heart valve thrombosis. *Circulation* 2015;8:e001596.
44. Martin C, Sun W. Simulation of long-term fatigue damage in bioprosthetic heart valves: effects of leaflet and stent

- elastic properties. *Biomech Model Mechanobiol* 2014;13:759–70.
45. Martin C, Sun W. Comparison of transcatheter aortic valve and surgical bioprosthetic valve durability: a fatigue simulation study. *J Biomech* 2015;48:3026–34.
 46. Li K, Sun W. Simulated transcatheter aortic valve deformation: a parametric study on the impact of leaflet geometry on valve peak stress. *Int J Numer Method Biomed Eng* 2017;33:e02814.
 47. Thubrikar MJ, Samanta S, Nolan SP. Optimization of a tri-leaflet valve design. *J Long Term Eff Med Implants* 1991;1:171–92.
 48. Mao WB, Li KW, Sun W. Fluid-structure interaction study of transcatheter aortic valve dynamics using smoothed particle hydrodynamics. *Cardiovasc Eng Technol* 2016;7:374–88.